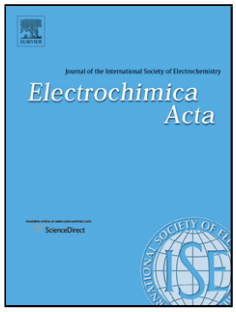

Title: Determining Electron Transfer Kinetics at Porous Electrodes

Author: <ce:author id="aut0005" author-id="S0013468617300105-497434e3975d9e563b1f8528df88c60f"> Jochen Friedl<ce:author id="aut0010" author-id="S0013468617300105-58ce884740813c05fcbe63819727cbb7"> Ulrich Stimming

PII: S0013-4686(17)30010-5
DOI: http://dx.doi.org/doi:10.1016/j.electacta.2017.01.010
Reference: EA 28677

To appear in: *Electrochimica Acta*

Received date: 31-8-2016
Revised date: 2-1-2017
Accepted date: 2-1-2017

Please cite this article as: Jochen Friedl, Ulrich Stimming, Determining Electron Transfer Kinetics at Porous Electrodes, Electrochimica Acta http://dx.doi.org/10.1016/j.electacta.2017.01.010

Determining Electron Transfer Kinetics at Porous Electrodes

Jochen Friedl[1], Ulrich Stimming[1,2,*]

[1] School of Chemistry, Bedson Building, Newcastle University, Newcastle upon Tyne NE1 7RU, United Kingdom

[2] TUM CREATE, 1 CREATE Way, #10-02 CREATE Tower, Singapore 138602, Singapore

* Corresponding author:

Tel.: +44 191 208 6786. E-mail address: ulrich.stimming@newcastle.ac.uk

Keywords: Porous electrodes, electrocatalysis, electroanalysis, vanadium, electrochemical impedance spectroscopy.

Abstract:

Porous carbon materials are of tremendous importance for electrochemical energy storage. Their low cost, wide potential window and high surface area make them ideal electrodes for many applications. The activity of the electrode towards a certain reaction is given by both the available wetted surface area and the electron transfer constant k_0. The present study investigates which electrochemical methods are suitable to determine k_0 on porous carbon electrodes. For this purpose, we investigate the ferric/ferrous redox couple on a porous carbon nanotube electrode as model system. We show that results from cyclic voltammetry (CV) can yield an apparent catalytic effect and elucidate its origin. Chronoamperometry and electrochemical impedance spectroscopy are shown to produce consistent values for the exchange current density I_0, which can then be normalized to k_0. Limitations of both

methods in terms of k_0 and diffusion constants are discussed.

The gathered insights in terms of validity of methods on porous electrodes are harnessed to review the recent literature on the vanadium redox reactions. Reported k_0 values spread over four orders of magnitude and there is no consensus on the influence of heat- or acid-treatment on the kinetics. Taking into account the difficulties of CVs on porous electrodes we conclude that reasonable values for the vanadium reactions are $k_0 < 1.2\ 10^{-4}\ cm\ s^{-1}$ and that oxidation of the samples increases surface area, catalyzes the V^{2+}/V^{3+} redox reaction but impedes the VO^{2+}/VO_2^{+} redox reaction.

Contents:

1. Introduction:

Porous carbon electrodes are ubiquitous in energy storage applications due to their high surface area (500 - 2000 m^2/g)[1]. They are employed as electrodes in supercapacitors as the capacitance increases

(mostly) linearly with the surface area accessible *A* to electrolyte ions[2]. In applications for which electron transfer is important, e.g. batteries or fuel cells, a high surface area *A* decreases the required current density *j* to achieve a current *I* and therefore reduces charge transfer overpotentials. Other advantages of porous carbon electrodes "include low cost, wide potential window, relatively inert electrochemistry, electrocatalytic activity for a variety of redox reactions"[3].

To increase the current that can be obtained from a battery electrode or fuel cell one has two options, either to increase the surface area *A* or to increase the exchange current density j_0. Enhancing j_0 is equivalent to increasing the catalytic activity of an electrode towards a reaction (or partial reaction) [4–7].

To assess whether a certain electrode composition, the size or dispersion of catalyst particles, the coordination of surface atoms or the substrate improve the catalytic activity of an electrode, j_0 has be determined unambiguously.

Electrochemical experiments, however, always yield the exchange current I_0, which is the product of *A* and j_0. Therefore, in order to determine either *A* or j_0, the other one has to be known.

On noble metal electrodes used for fuel cells there a number of experimental methods to determine the electrochemical active surface area *A* [8,9]: H_2 adsorption and desorption and CO and Ag deposition.

For high surface area carbons the gases typically chosen for adsorption studies are N_2 or CO_2[10]. Watt-Smith et al. found a good correlation between the surface area A^{BET} determined from the Brunauer-Emmett-Teller (BET) method and values obtained from small-angle X-ray scattering for two out of three carbon samples with $A^{BET} \leq 796\ m^2\ g^{-1}$ [10]. Interaction of chemical species with the adsorbing gas led to complex surface layers and A^{BET} could not be determined for one of the samples [10]. For very high surface area carbons, from around $A^{BET} = 1000\ m^2\ g^{-1}$, the surface area accessible to the electrolyte becomes almost constant whereas A^{BET} can increase further [1]. As the size of molecular probes used in BET experiments (N_2, CO_2) differs from the size of solvated ions in the electrolyte a discrepancy between *A* and A^{BET} is not surprising.

Another possibility to determine A is via the double layer capacitance C_{DL} and the specific capacitance of the electrode material c_{DL} [F/cm^2]. Values for c_{DL} are given in the literature ($< 2\mu F/cm^2$ for basal plane HOPG, $\sim 60\ \mu F/cm^2$ for edge plane HOPG and $24\text{-}36\ \mu F/cm^2$ for GC[3,11,12]) and can be used to determine A by dividing C_{DL} by c_{DL}. Two caveats exist to this method: First, the ratio between edge plane and basal plane might be unknown, and therefore the large difference between the two values makes a recalculation difficult. Second, the C_{DL} is potential dependent which is not considered in above literature values[13].

Microscopy techniques such as tapping mode atomic force microscopy[14] and scanning tunneling microscopy can be used to obtain an image of the electrode surface and then deduct the roughness from it[15], but these tools will not reveal the porosity of the bulk of the electrode interior.

Determination of I_0 on porous electrodes is also not a simple task. A number of studies showed that porosity and surface alter electrochemical responses compared to flat model electrodes [16–22]. The planar diffusion model does not hold and it was stated that the electrode effectively does not have a constant active surface area A[21]. However, one could also argue that there is a dispersion of diffusion coefficients and this is responsible for the inapplicability of textbook electrochemical equations: The high surface area electrode material hinders diffusion of redox species from the bulk electrolyte into the pores. With distance from the outer electrolyte-electrode interface, deeper within the porous structure, the diffusion constants will decrease. Porosity might further influence the effective viscosity of electrolyte[23]. Therefore, to determine I_0 on porous electrodes, a measurement technique has to be chosen that has access to a time regime in which the redox species within the pores are not depleted yet and therefore diffusion plays a negligible role. In general, both the redox kinetics and the mass transport contribute to the overpotential for a given redox reaction. In practical electrochemical energy storage or conversion devices it is crucial to obtain reaction conditions under which both kinetics and mass transport are fast.

However, the presented study only deals with the determination of the electron transfer constant k_0 in a time regime in which mass transport limitation is less important. For the combined treatment of both kinetics and mass-transport in electrochemical cells the reader is referred to other studies[24–30].

In this study, we will investigate a model system, the ferric/ferrous couple on a multi-walled carbon nanotube (MWCNT)-modified GC electrode, to obtain and compare values for I_0 from three different measurement techniques: Cyclic voltammetry (CV), chronoamperometry (CA) and electrochemical impedance spectroscopy (EIS). Possible ways to obtain A and therefore j_0 and the electron transfer constant k_0 are discussed then. We will also present a method that normalizes the charge transfer resistance R_{CT} by the C_{DL}, both values are obtained from EIS [17].

With the insights obtained regarding the suitability of CV, CA and EIS for porous electrode materials we will review the recent literature on the kinetics of the vanadium redox reactions (V^{2+}/V^{3+} and VO^{2+}/VO_2^{+}). These two redox reactions are employed in the commercially important All-Vanadium Redox Flow Battery (VRB)[31,32] and are mostly investigated on porous electrodes. In the literature, k_0 values for these two redox reactions spread over four orders of magnitude (see Fig. 5) and we will review how these strongly deviating values were obtained[33–35]. The additional benefit when combining the study on the electrochemical techniques and the review on the vanadium redox reactions is that we will be able to show that this discrepancy in k_0 values can be explained by the selection of electrochemical techniques unsuitable for high surface area carbon electrodes.

2. Comparison of experimental methods to obtain kinetic information on porous electrodes

2.1 Experimental methods and materials

To generate porous electrodes MWCNTs NC3100 from Nanocyl were deposited onto glassy carbon electrodes as reported previously [17]. Variable amounts of MWCNTs were suspended in Hexane and

ultrasonically dispersed. With a pipette *20 µl* of this solution was then drop-cast onto glassy carbon facets and dried at 55˚C until the solvent was evaporated. Repetition of this coating process led to higher amounts of MWCNTs on the electrode.

The electrolyte comprised *50 mM* Fe^{2+} (*$FeCl_2$ 4 H_2O*, Sigma-Aldrich, reagent grade) and *50mM* Fe^{3+} (*$FeCl_3$ 6 H_2O*, Sigma-Aldrich, reagent grade) in *1 M* H_2SO_4 (Sigma-Aldrich, Suprapur).

A gold wire served as counter electrode and a Mercury/Mercourus Sulfate in *1 M* H_2SO_4 (MSE, *0.674 V* vs. the Standard Hydrogen Electrode (SHE) [36]) was employed as reference electrode. All potentials are given recalculated to SHE. Prior to each measurement the electrolyte was purged with Argon in a custom built cell and kept under Argon for the duration of the experiment. A SP300 from Bio-Logic was used as potentiostat. Simulations of CVs were performed with the EC-Lab v11.02 software by Bio-Logic.

In this section, three electrochemical methods are compared. The working electrode is a porous MWCNT structure on glassy carbon and the redox system under investigation is *50 mM* Fe^{2+} and *50 mM* Fe^{3+} in *1 M* H_2SO_4. For CV, CA and EIS the raw data will be presented and it will be discussed how the exchange current I_0 can be obtained from these measurements. After that I_0 will be converted to k_0 by estimating the surface area by using BET and the specific capacitance.

2.2. Cyclic voltammetry

CVs of *50 mM* Fe^{2+} and *50 mM* Fe^{3+} on a polished glassy carbon (GC) electrode (orange curve), on GC with *1 µg* MWCNTs (green curve) and with *4 µg* MWCNTs (blue curve) are shown in Fig. 1a. The equilibrium potential of the ferric/ferrous redox couple is obtained by adding the potential positions of the anodic and cathodic peak of the orange curve and dividing by 2, i.e. *U_0 = 0.68 V vs. SHE*. The sulfate ions in the supporting electrolyte are responsible for this shift from the characteristic standard potential *$U^{\ominus}$ = 0.77 V vs. SHE* [17,37,38]. The orange curve, recorded on a relatively flat, polished GC electrode, shows a current peak for the oxidation from Fe^{2+} to Fe^{3+} at $U_{ox}^{peak} = 0.88\ V$ and the peak for the corresponding reduction at $U_{red}^{peak} = 0.47\ V$. On GC with *1 µg* MWCNTs there are two oxidation peaks at $U_{ox,1}^{peak} = 0.75$

V and $U_{ox,2}^{peak} = 0.87$ V and two reduction peaks at $U_{red,1}^{peak} = 0.62\ V$ and $U_{red,2}^{peak} = 0.44\ V$. On the GC substrate decorated with *4 µg* MWCNTs there are again only 2 peaks, one for the oxidation at $U_{ox,1}^{peak} = 0.74\ V$ and one for the reduction at $U_{red,1}^{peak} = 0.63\ V$.

Our interpretation is that the peaks with a wide potential separation (orange curve and U_2^{peak} green curve) originate from the flat GC, whereas the peaks with a small peak separation (blue curve and U_1^{peak} green curve) are generated by the MWCNTs, the porous part of the electrode. The green curve shows both types because *1 µg* of MWCNTs is not sufficient to cover the entire surface of the GC substrate. With the above hypothesis, that there are peaks on porous parts of the electrodes and peaks on flat electrodes, established, the question remains why porous and flat structures generate different signals. Keeley et al. stated that the surface area during the course of a CV changes on porous structures[21]. In our opinion, it would be better to speak of a dispersion of diffusion coefficients, which then leads to a current response that is unexpected when only linear diffusion is considered. In order to exemplify this, we modeled the CV response of two redox systems. The reference system has a surface area of A^1 (orange curve in Fig. 1b), while the porous system has the tenfold surface area, but a diffusion coefficient that is 0.01 times the value of the other (blue curve). In a cartoon of the electrode and its active surface area (Fig. 1c), the blue curve is recorded within the porous structure, while the orange curve is recorded on the flat part of the electrode and on the outside of the porous structure. Pores can generate a big surface area (10 A^1), but diffusion of redox species from the bulk is considerably hindered by the carbon structure (0.01 D^1). The shape of the simulated curves in Fig. 1b shows that the small diffusion coefficients yield CVs with a smaller peak separation than bigger diffusion coefficients. The difference in surface area ensures that the currents of the blue and orange curve are similar. Considering that the peak position is determined by an interplay of Butler-Volmer kinetics and the onset of mass transport limitation [38], the influence of the diffusion coefficient can be understood.

Extraction of kinetic information from CVs is typically performed via the peak separation $\Delta U = (U_{ox}^{peak} - U_{rd}^{peak})$. CVs recorded with various scan-rates on the sample with 4 µg of MWCNTs are shown in Fig. 2a. It can be observed that the peaks become less defined for faster scan-rates. This can be expected, as the MWCNT – GC system is complex and diffusion coefficients should vary for different locations in the electrode. Also, a dispersion in ohmic resistance is expected for the various parts of the electrode and therefore the electrode potential $U_{electrode} = U_{applied} - I\,R_{Ohm}$ will vary throughout the electrode. The peak separation between $U_{ox,1}^{peak}$ and $U_{red,1}^{peak}$ is shown for samples with 1 and 4 µg of MWCNTs in Fig. 2b. For both samples, the peak separation increases with scan-rate and the electrode with 4 µg of MWCNTs and therefore the higher surface area exhibits a smaller peak separation than the other sample. We converted these peak separations to k_0 values by simulating CV with a diffusion constant $D = 5.6\ 10^{-6}\ cm^2\ s^{-1}$ for both Fe^{2+} and Fe^{3+} [39]. These k_0 values are shown in Fig. 2c and it can be seen that we do not obtain constant values, but that in fact on electrodes with higher porosity a a higher "k_0" is determined and that the determined electron transfer constants k_0 increase with higher scan-rates. This indicates that ΔU on porous structures depends on the geometry of the electrode as well as on the electron transfer constant k_0[40].

Punckt et al. meticulously studied CVs on electrodes prepared by drop-casting carbon nanomaterials [16,40,41]. Their verdict was that due to electrode porosity "only effective, i.e., morphology-related, reaction kinetics can be determined from CVs but not the intrinsic electrochemical kinetics of the electrode material." [40].

2.3 Electrochemical impedance spectroscopy

EIS was performed at the rest potential which matched the U_0 of the ferric/ferrous redox reaction. Nyquist plot and Bode plot *of 50 mM* Fe^{2+} and *50 mM* Fe^{3+} on an electrode with *1 µg* of MWCNTs are shown in Fig. 3. The equivalent circuit used was the standard Randles-circuit with a constant phase

element (CPE) given in Fig. 3 [42]. The CPE was converted to a double layer capacitance (C_{DL}) by the formula given by Hirschorn et al. for a surface distribution [43]:

$$C_{DL} = Q^{\frac{1}{a}}\left(\frac{R_{Ohm}\,R_{CT}}{R_{Ohm} + R_{CT}}\right)^{(1-a)/a} \quad (1)$$

With the ohmic resistance $R_{Ohm} = 3.8\ \Omega$, charge transfer resistance $R_{CT} = 11.4\ \Omega$, $Q = 0.16\ 10^{-3}\ F\ s^{(a-1)}$ and $a = 0.8$ we obtain $C_{DL} = 23.4\ 10^{-6}\ F$. The exchange current I_0 is inversely proportional to R_{CT} and can be obtained as $I_0^{EIS} = 2.3\ mA$.

The maximum k_0 that can be determined by EIS depends on the highest frequency ω which can be measured and the diffusion constant [44]. The requirement is that R_{CT} cannot be small compared to the Warburg impedance:

$$R_{CT} \geq \frac{1}{5}\left[R_W^2 + \left(\frac{1}{\omega C_W}\right)^2\right]^{1/2} \quad (2)$$

With the resistive R_W and capacitive C_W component of the Warburg impedance .This can be simplified to (see supplementary information):

$$\frac{1}{k_0} \geq \frac{2}{5}\frac{1}{\sqrt{\omega D}} \quad (3)$$

This means that EIS can determine electron transfer constants $k_0 \leq 0.025\ cm\ s^{-1}$ even for very small diffusion constant $D = 10^{-8}\ cm^2 s^{-1}$, brought about by the porous structure, provided that frequencies of $10^5\ Hz$ are accessible. The maximum frequency that can be applied depends very much on the cell geometry and on the specific resistivity of the electrolyte [45,46].

2.4 Chronoamperometry

Chronoamperometry (CA) is a method that perturbs the potential of an electrode from U_0 or another rest potential and measures the time-dependent current.

The faradaic current can be calculated by an expression containing a term for Butler-Volmer (BV)-

kinetics and a term that contains the depletion of active species at the electrode [47]. When judging whether CA can be used to investigate I_0 on porous electrodes one has to look at the time regimes the measurement can give access to. At very short times the double layer capacitance of the electrode-electrolyte interface is charged, this non-faradic current masks the faradaic current. After $5\ (R_{Ohm}\ C_{DL}) = 0.67\ 10^{-3}$ s (R_{Ohm} and C_{DL} from EIS) this non-faradaic current has fully decayed. At the other end of the time spectrum, for the current to have any sensitivity to kinetic control and not be dominated by mass-transport, E. Yeager and J. Kuta gave the formula [44]:

$$k_0 \leq 2.5\ (D/t)^{1/2} \tag{4}$$

Therefore, with and $D = 5.6\ 10^{-6}\ cm^2/s$ [39] and $k_0 = 5\ 10^{-3}\ cm/s$ [48] the time regime of CA which yields kinetic information for the MWCNT – Fe^{2+}/Fe^{3+} system can be estimated to:

$$0.67\ 10^{-3}\ s < t < 1.5\ s \tag{5}$$

This time regime seems to be sufficient to detect the kinetic current. However, as we have seen in the CV-section, diffusion constants might be significantly smaller in porous structures, hence reducing the maximum time limit.

For the evaluation of experimental data we follow the extrapolation method given by H. Gerischer [49]. Fig. 4a shows anodic potential steps from the resting potential $U = 0.68\ V$ vs. SHE. The bottom abscissa gives the square-root of time, whereas the top abscissa gives linear time. Potential steps for several overpotentials from *20 mV* to *200 mV* are shown. Three time regimes can be discerned:

1. $0 < t < \sqrt{0.02s}$ ($\triangleq 4\ 10^{-4}\ s$): In this time regime an exponentially decaying current can be seen. This corresponds to the contribution from the double layer charging, the observed current is a

mix of faradaic and non-faradaic currents. Note the similarity to *5 (R_{Ohm} C_{DL})= 4.4 10^{-4} s* obtained from EIS;

2. $\sqrt{0.02s}$ < t < $\sqrt{0.055s}$ *(≙3 10^{-3} s*): In this time regime the kinetic current can be observed. It decays due to the diminishing concentration of oxidizable species (*Fe^{2+}*). Extrapolating this curve to *t = 0s* yields the kinetic current corresponding to the applied overpotential.
3. t >$\sqrt{0.055s}$ *(≙3 10^{-3} s*): In this time regime the current is mass-transport limited and therefore dependent on *D* and not I_0.

A plot of all extrapolated data points *I(t=0s)* for anodic and cathodic overpotentials is shown in Fig. 4b. Extrapolation of those points to zero overpotential gives the exchange current $I_0^{BV} = 1.5\ mA$ (the mean of the values obtained from anodic and cathodic branch was assumed). According to the Butler-Volmer equation the slopes m_{an} and m_{cat} are:

$$m_{an/cat} = \alpha_{an/cat} \frac{F}{RT} \tag{6}$$

With Faraday constant *F*, gas constant *R*, absolute temperature *T* and anodic (α_{an}) and cathodic (α_{cat}) symmetry factors. Therefore CA yields α_{an} *= 0.50* and α_{cat} *= 0.46* in addition to the value for I_0^{CA}.

An alternative, microscopic theory of electron transfer based on the work of Marcus can be used instead of the empiric Butler-Volmer model for outer-sphere electron transfer[50,51]. With expansion from Chidsey [52] the theory is now known as Marcus-Hush-Chidsey (MHC) model[53]. Bazant and co-workers simplified the formula for current vs. overpotential so that the MHC evaluation can now be as easily performed as the analysis according to the BV model[54,55]. The resulting fit for the MHC – model is also shown in Fig. 4b. The curve was calculated using equ. 18 from the publication by Zeng et al. [54]. The determined reorganization energy $\lambda^{MHC} = 0.18\ eV$ is much than theoretical values for the same redox couple, $\lambda^{DFT} = 2.11\ eV$ [56] , but is similar to experimental values for the *Fe^{2+}/Fe^{3+}*

redox reaction in $LiFePO_4$ electrodes, $\lambda^{LiFePO_4} = 0.21\ eV$ [57]. The obtained exchange current is $I_0^{MHC} = 1.6\ mA$.

2.5 Comparison of methods and normalization to surface area

Employing CV, EIS and CA on a porous electrode we have obtained values for I_0 from two methods, EIS and CA.

To normalize I_0 to k_0 we have to estimate the surface area of the MWCNT coated electrodes. One method is to use the specific capacitance of carbon materials, estimated at c_{DL} =5 $\mu F\ cm^{-2}$ [3], and then divide C_{DL} by c_{DL}. This yields $A^{CDL} \approx 4.6\ cm^2$.

Another option is to use the literature value for the BET surface area of NC3100 MWCNTs, *334* $m^2\ g^{-1}$ [58]. As we have put *1* μg of MWCNTs on a polished glassy carbon electrode with radius *0.5 mm*, the surface area from BET in addition to the polished substrate is $A^{BET} \approx 3.3\ cm^2 + 0.79\ cm^2 = 4.1\ cm^2$.

Values for k_0 for the Fe^{2+}/Fe^{3+} redox reaction on the MWCNT modified electrode are given in table 1. The redox reaction is sensitive to the presence of surface oxides, particularly carbonyl groups[3]. This makes it difficult to judge whether our presented methods produced "correct" values for k_0. Hung and Nagy reviewed 13 studies about the kinetic data of the ferric/ferrous redox reaction and found values $1.3\ 10^{-4}\ cm\ s^{-1} < k_0 < 2.3\ 10^{-2}\ cm\ s^{-1}$ on Pt electrodes[48]. However, as the redox reaction is catalyzed by chloride ions, they extrapolated the data to a "chloride free" electron transfer constant of $k_0 = 2.5\ 10^{-5}\ cm\ s^{-1}$. Our rates are higher than this lower limit, which can be explained by the catalytic effect of surface functional groups on the NC 3100 MWCNTs (2.2 weight% as determined from thermogravimetric analysis [17]).

Which method, CA or EIS, is preferred is up to the experimentalist to decide, both methods are suitable on porous electrodes. However, EIS has advantages in terms of simplicity and speed of data acquisition. For CA multiple potential steps have to be recorded and evaluated. For EIS only a single impedance spectrum has to be recorded and then fitted to an equivalent circuit. On the other hand, CA yields the

additional information of the transfer coefficients α_{an} and α_{cat}.

Another fact to keep in mind is that in high surface area carbon electrodes the ohmic drop within the electrode phase can lead to a dispersion of potentials which is then problematic for electrochemical measurements. This is especially true for high current conditions [59]. Therefore, as overpotentials and therefore currents are lower in EIS than in CA measurements, the former might be more suitable to avoid a poor electrode potential distribution during the measurement. Another advantage of EIS is that impedance distributions or transmission lines can be employed to fit the experimental data[42].

Comparison of electron transfer constants determined from CVs with Table 1 shows that CVs give values that are at least ten times higher than k_0 determined from EIS or CA. The dispersion of diffusion constants experienced in CV makes it very difficult to extract kinetic information.

For comparison of the activity of various electrode materials for one redox reaction, our group has developed a technique based on EIS [17]. It can also be employed to compare the activity of multiple redox reactions on electrodes if the normalization is done properly [13]. This technique is very similar to the normalization of I_0 by the C_{DL}, it relies on the fact that both C_{DL} and R_{CT} are proportional to A[38]:

$$R_{CT} = \frac{RT}{n\,F\,A\,j_0} \tag{7}$$

The formula of C_{DL} depends on the geometry of the electrode (planar, tubular, spherical…), but it can be approximated as[60]:

$$C_{DL} = \varepsilon_0 \varepsilon_r \frac{A}{t_{DL}} \tag{8}$$

With the thickness of the double layer t_{DL}, the dielectric constant ε_0 and the relative permittivity ε_r. It is important to note that ε_r in the first water layer at an electrode might be significantly smaller than the bulk value of roughly 80 [17,61–63]. Substituting for the unknown A equations 7 and 8 can be combined to[14]:

$$R_{CT}^{-1} = \frac{nFt_{DL}}{RT\varepsilon_0\varepsilon_r} j_0 C_{DL} \quad (9)$$

Employing electrodes of the same composition but various sizes then yields a linear relation between R_{CT}^{-1} and C_{DL} and from the slope the kinetic information j_0 or k_0 can be determined [13,17]. This method is based on the same principle as the normalization of EIS data by specific capacitance c_{DL} values as described above, but has the advantage that the result is more graphical and the influence of the substrate can be identified and subtracted.

Another method to determine charge transfer kinetics on porous electrodes, not presented here, is based on flow through configurations [22,64,65]. It is similar to rotating disk electrodes as the flow of electrolyte reduces the influence of mass-transport limitation, but this technique has the advantage that it emulates the use of the electrode in an actual electrochemical device.

3. Electron transfer kinetics of the vanadium redox reactions - a review

A set of redox reactions for which the porous carbon electrodes are of immense importance are the vanadium redox reactions[28]:

$$V^{2+} \leftrightharpoons V^{3+} + e^- \qquad U^{\Theta,1} = -0.26\ \text{V vs. SHE} \quad (10)$$

$$VO^{2+} + H_2O \leftrightharpoons VO_2^+ + 2H^+ + e^- \qquad U^{\Theta,2} = 1.00\ \text{V vs. SHE} \quad (11)$$

These redox reactions constitute the anolyte (eq. 10) and catholyte (eq. 11) of the All Vanadium redox flow battery (VRB). If a current is drawn, the voltage *V* of the VRB is given by[26]:

$$V = U^{\Theta,2} - U^{\Theta,1} - |\eta_{ct}^c| - |\eta_{ct}^a| - |\eta_{diff}^c| - |\eta_{diff}^a| - I\,R_{Ohm} \quad (12)$$

With reaction overpotentials $\eta_{ct}^{c/a}$ at the cathode and anode, the diffusion overpotential $\eta_{diff}^{c/a}$ at cathode and anode and the voltage drop caused by the sum of all electronic and ionic resistances

$I\,R_{Ohm}$[66].

The charge transfer overvoltage η_{CT} is directly tied to the exchange current density of the employed redox reactions and through the Butler-Volmer Equation (assuming $R_{ohm} = 0$):

$$I = j_0 A[\frac{c_O(0,t)}{c_O^*}\exp(\frac{\alpha_{cat}F}{RT}\eta_{CT}) - \frac{c_R(0,t)}{c_R^*}\exp(-\frac{\alpha_{an}F}{RT}\eta_{CT}) \quad (13)$$

With concentrations of oxidized (c_O^*) and reduced (c_R^*) species. This means that in order to achieve a small η_{CT} at a given current *I* the product of j_0 and *A* has to be high. This is precisely the reason why for RFB applications high surface area, porous electrodes are favored. However, arguably more important than *A* is j_0 or k_0, as values for k_0 can spread over several orders of magnitude. For example, the ferrocene/ferrocenium redox couple is often attributed an electron transfer constant of $k_0 \approx 1$ cm s^{-1} [67], while for the VO^{2+}/VO_2^+ redox reaction $k_0 \approx 3\ 10^{-7}\ cm\ s^{-1}$ was determined on graphite [68]. Therefore, catalysis of the latter reaction, as well as for the one taking place in the anolyte of the VRB, is a hot topic in the literature. In Table 2 we compiled a list of recent studies that determined k_0 values for the vanadium reactions on porous carbon electrodes. Studies on non-porous electrodes[69,70] and studies that look at porous structures but do not give an explicit value for k_0 or j_0 [13,71–77] were ignored for this compilation.

The data points from Table 2 are also plotted in Figure 5. It is striking that the values for k_0 for both redox reactions spread over four orders of magnitude, and this is only accounting for studies published from 2011 to 2016. Another interesting detail of the graphs is that for the V^{2+}/V^{3+} redox reaction (Fig. 5b) the trend for the influence of oxidation/reduction of the electrode material, be it electrochemically, chemically or thermally, is uniform throughout the listed studies. This is not the case for the VO^{2+}/VO_2^+ redox reaction: Two studies assign faster kinetics to oxidized samples [35,78], while two studies conclude that reduced samples show larger values for k_0 [17,79].

This situation is unsatisfactory and we will apply the knowledge obtained in part 1 of this paper, how to determine the electron transfer constant on porous electrodes, to critically discuss the studies listed in Table 2.

Jelyani et al. modified a piece of carbon felt (CF) with carbon nanotubes (CNTs), chemically oxidized the material in 98% sulfuric acid and then placed it in a furnace at either *250 ˚C* or *450 ˚C* [78]. The influence of heat treatment on carbon felt electrodes has recently been studied intensively [83,84]. Chemical oxidation of carbons with acids is expected to follow a two-step process[85]: First, defects are generated when the oxidant attacks the carbon structure by electrophilic reactions which generates active sites such as *–OH* and *–C=O*. Second, under very oxidizing conditions, especially on CNTs, the graphene structure around the defect is broken and thereby the defect is removed from the electrode. This second step can be observed as mass loss of the CNTs [86] and has also been seen by Jelyani et al. [78]. Fourier Transform Infrared Spectroscopy (FTIR) spectra are shown that suggest that the heat and acid treatment generated functional groups on the CF-CNT electrode [85,87,88]. The hydrophilicity of the carbon electrodes was determined by comparing the weight of dried and wet samples. It was found that an acid- and heat-treated CF-CNT sample can absorb *1237 wt%* of water, whereas the untreated CF-CNT sample can only absorb *69 wt%*. This suggests that the introduced functional groups increased the hydrophilicity of the electrode, as reported previously [13,89].

Kinetic information on the V^{2+}/V^{3+} and VO^{2+}/VO_2^{+} redox reaction was obtained by EIS at the open circuit potential of equal concentrations of the redox couples. Obtained values for R_{CT} were converted to j_0, we recalculated those to k_0 and listed them in Table 2. From the values, it can be seen that the authors attribute a *24* fold increase in k_0 for VO^{2+}/VO_2^{+} to the acid treatment and an acceleration of a factor of *18* for the V^{2+}/V^{3+} redox reaction. However, to obtain j_0 from R_{CT} the geometric surface area of the electrode ($1\ cm^2$) was used for all samples. The stark contrast in wettability (1237 wt% / 69 wt% ≈ 18)

between treated and untreated sample suggests that the seen effects in R_{CT} stem from the increased surface area *A* and not from the exchange current density j_0 as stated.

Miller et al. employed a single strand of carbon fiber with a thickness of approximately *15 µm* as electrode [79]. Contacted by sealed wires only the fiber was exposed to the vanadium electrolyte. While this is not technically a porous electrode, it is included in this review because the experimental setup presents a way to extract reaction kinetics for a material that is typically employed as a porous, 3D electrode. The single fiber, a carbon fiber microelectrode (CFME), was then exposed to oxidizing (*2.2 V, 2.0 V, 1.7 V* vs. SHE[1]) or reducing potentials (*0.2 V, -0.2 V, -1.3 V* vs. SHE) and analyzed by x-ray photoelectron spectroscopy (XPS); oxidative potentials increased the oxygen to carbon ratio from *0.34* for the untreated sample, whereas reductive potentials reduced it.

The activity of the treated and untreated CFME towards both vanadium redox reactions was investigated by linear sweep voltammetry (LSV, scan-rate *5 mV* s^{-1}, and EIS. Some exemplary values for k_0 are given in Table 2 and Fig. 5. The specific double layer capacitance c_{DL} of the fiber was determined from CVs and it is assumed that the authors use this value to normalize the kinetic information. The authors conclude that oxidative treatment of the CFME has a positive effect for the V^{2+}/V^{3+} redox reaction, with a transfer constant an order of magnitude greater after treatment at *2.2 V* than at *-1.3 V*. Diametrically, the transfer constant of VO^{2+}/VO_2^{+} was about four times greater after treatment at *-1.3 V* than after that at *2.2 V*. The authors further state that the kinetics of VO^{2+}/VO_2^{+} are significantly faster than of V^{2+}/V^{3+}. However, from the paper it is not clear if the authors considered the variable c_{DL} at the potentials of the two vanadium reactions in their comparison. On carbon felt electrodes the c_{DL} is roughly a factor of 2 larger at potentials around *1 V* vs. SHE than at *-0.25 V* vs. SHE [13]. Nevertheless, the Miller et al. clearly showed the dependence of k_0 on the oxygen content of a single carbon fiber and further stated an important insight for the future development of VRBs: The potential under which the

[1] Values recalculated from the MSE assuming a potential of 0.67 V vs. SHE[13]

low potential half-cell operates is equivalent to the applied reduction potentials in the study. Therefore, during operation conditions the electrode of the low potential half-cell is kept in a potential region which leads to deactivation (both surface area A and activity k_0) of the electrode towards the V^{2+}/V^{3+} redox reaction[79].

As we have seen CVs, and therefore also LSVs face challenges to determine k_0 on porous electrodes due to mass transport problems into the porous structure. Goulet et al. found a way around this limitation by using a flow-through configuration [65]. The authors placed a porous carbon paper electrode (*A = 4 m^2/g*) in a stream of 1.7 M commercial grade vanadium solution with equal concentrations of oxidized and reduced species. Employing variable flow rates (from *2* to *2000 µL min^{-1}*) the potential of the working electrode was perturbed from the open circuit potential to $\eta = \pm 200\ mV$, the resulting Tafel curves were corrected for the IR_{Ohm} drop (determined from EIS) and used to extract I_0. As given in Table 2 values of $k_0 = 1.8\ 10^{-5}\ cm\ s^{-1}$ for the VO^{2+}/VO_2^{+} redox reaction, and $k_0 = 2.4\ 10^{-7} cm\ s^{-1}$ for the V^{2+}/V^{3+} were determined[65]. The authors concluded that at sufficiently high flow rates, Tafel analysis can be performed without the need for mass-transport corrections. Estimation on how this *sufficiently high flow rate* depends on k_0 would be highly interesting as it can be expected that the flow rate will have to increase to investigate more facile redox reactions.

Employing eq. 7 our group determined R_{CT} and C_{DL} of CNTs with various degrees of functionalization and thereby obtained a value for the expression $\frac{nFt_{DL}}{RT\varepsilon_0\varepsilon_r} j_0$ which is independent of the surface area *A* as shown in Fig. 6 [17]. The untreated CNTs are as described in section 2.1, CNT reduced were heated to *1000 ˚C* in Argon atmosphere for *3h*, CNT oxidized were treated in conc. H_2SO_4/conc. HNO_3 for *6 h*. The used glassy carbon substrate, given as empty black circle in Fig. 6, shifts all lines from the origin. Conversion of the slopes to a quantitative k_0 was done by extracting t_{DL} and ε_r from the slope of GC electrodes with various sizes, and the assuming that $k_0^{GC} \equiv 3\ 10^{-7}\ cm\ s^{-1}$ [90]. This gave a value for $\frac{t_{DL}}{\varepsilon_r} = 2.2\ 10^{-11}\ m$

which yielded a reasonable value of the thickness for the innermost layer of water of $t_{DL} \approx 2$ Å [17,61,62]. This results in k_0 values for the CNTs on the order of 10^{-6} cm s^{-1}, with higher values for less oxidized samples. This was the first study that showed that functional groups are detrimental for the VO^{2+}/VO_2^+ redox reaction, which has since then been confirmed by multiple studies [13,69,79,91].

R. Schweiss investigated polyacrylonitrile-based carbon felts[80]. By modifying the carbonization protocol two more felt types besides the commercially available Sigracell® GFD 4.6 by SGL Carbon GmbH were produced. This resulted in felts with different surface area (BET, 266 – 176 roughness factor), geometry and chemical composition (XPS, N content from 3.6% to 0.1%). Kinetic information was obtained by looking at the peak separation in CVs [38]. As the porosity of the felts influences the peak position in CVs the exact values for k_0 are somewhat questionable, however, the highest determined k_0, as well as the highest voltage efficiency in a full VRB, was found for felts with a moderate degree of graphitic order and a bulk nitrogen content of about *2%*. Nitrogen and nitrogen-containing functional groups offer a design space that has not been explored sufficiently for VRB electrodes, most studies focused on oxygen-containing functional groups [71,92].

Agar et al. performed CV measurements on untreated, heat- (400 ˚C for 6h in air) and acid-treated (98% sulfuric acid for 6h) carbon felt electrodes [35]. Electron transfer constants were determined via CVs, and heat- and acid-treated electrodes were found to exhibit higher k_0 values than pristine electrodes for both half-cell reactions. Problematic, besides the apparent catalytic effect observed in CVs, is the fact that the surface area was taken as the geometric surface area and that it was assumed that the treatment does not alter the surface area. However, both oxidative methods have been reported to increase the surface area [13,78,89].

Wu et al. compared carbon paper electrodes with pyrolytic graphite and glassy carbon for both vanadium reactions [81]. The electrochemical analysis was performed with CVs. Whereas the flat

electrodes showed a large peak separation (> 0.9 V), the carbon paper exhibited a peak separation of only 0.227 V. The electron transfer rate on GC was then determined as k_0^{GC} = 5.4 10^{-5} cm s^{-1} and on carbon paper as k_0^{CP} = 1.13 10^{-3} cm s^{-1} for the V^{2+}/V^{3+} redox reaction. Similar values were reported for the VO^{2+}/VO_2^{+} redox reaction. The increased activity was then assigned to the large surface area and to a postulated inner-sphere mechanism for the reaction on the carbon paper electrode[81]. The former argument is invalid, as the electron transfer constant is normalized to surface area, and for the second it is not clear why the carbon of a carbon paper electrode should behave differently than that of pyrolytic graphite, similar to the argument against the high intrinsic redox activity of graphene [16,19].

A similarly high electron transfer constant of k_0 = 1.3 10 cm s^{-1} was reported by Mazurenko et al. on macroporous CNT-carbon composites for the VO^{2+}/VO_2^{+} redox reactions [82]. The surface area was determined using the Randles-Sevcik equation, assuming a diffusion constant that was obtained on flat electrodes [93]. In addition, the authors also recorded the C_{DL} for their samples, and when using the apparent surface area obtained from CVs they found specific capacitances ranging from c_{DL} = 10.8 mF cm^{-2} to c_{DL} = 199 mF cm^{-2}. This indicates that employing the Randles-Sevcik equation underestimates the electrochemical surface area and therefore, together with the limitations of CVs on porous structures the reported k_0 values are too high.

In summary, considering how difficult it is to extract k_0 on porous structures with CVs, three of the studies listed in Table 2 employ a more suitable method and succeed in separating contributions from surface area and electrochemical activity[17,65,79]. As can be seen in Fig. 5 these are all studies that place the electron transfer constant in the lower end of the spectrum which spans from 10^{-7} cm s^{-1} to 10^{-3} cm s^{-1}. Also, while the k_0 values for the VO^{2+}/VO_2^{+} redox reaction determined in studies [17,79] are separated by one order of magnitude, both studies describe the influence of oxygen-containing functional groups in a similar way: Oxygen-containing functional groups impede the VO^{2+}/VO_2^{+} redox reaction[69,91], regardless

of the increase in surface area with increasing functionalization [13]. Combining X-ray absorption fine structure studies with our electrochemical results we hypothesized that vanadium oxides (VO_x) chemisorb on the oxygen functional groups and that these VO_x species passivate parts of the electrode[13,94]. It is plausible that this chemisorption is potential dependent and therefore hinders only the VO^{2+}/VO_2^+ redox reaction at high potentials, whereas the V^{2+}/V^{3+} redox reaction at low potentials remains unaffected by these vanadium oxides.

The question of which half-cell reaction has the higher k_0 was answered by Miller et al.: Oxidized carbon has a similar activity for both reactions, with reduction of the electrode the kinetics slow down for V^{2+}/V^{3+} and accelerate for VO^{2+}/VO_2^+ [79]. We reported a similar statement, albeit without calculating k_0: That the composition of the electrode determines which half-cell reaction has the higher electron transfer constant [13]. An interesting avenue of research has been opened by a study incorporating the nitrogen content, which could have different catalytic properties than oxygen content and should be investigated in the future[80].

4. Conclusions

In the first part of this study, we have shown that CVs are not a suitable tool to determine electron transfer constants on porous structures. A changing surface area and a dispersion of diffusion coefficients during the applied potential ramp make it so that the peak potential depends on the electrode porosity, and not on the kinetics of the redox reaction[16,17,21,22,40,41]. On the other hand, EIS and CA can be used to determine I_0 on porous structures and we have presented expressions for the maximum k_0 that can be detected. With both techniques, the transition from kinetic to mass-transport control can be directly observed. In order to calculate k_0 from I_0 the surface area A has to be known. We compared results for A determined from BET and the double layer capacitance C_{DL} and could conclude that both methods yield similar results. For the model redox system Fe^{2+}/Fe^{3+} on a porous MWCNT electrode, we found electron transfer constant in the range of

$7.6\ 10^{-5} cm\ s^{-1} < k_0 < 1.2\ 10^{-4}\ cm\ s^{-1}$. This is a reasonable result, considering that the minimum k_0 under non-catalytic conditions is $k_0 = 2.5\ 10^{-5}\ cm\ s^{-1}$ [48].

With this information on the validity of various electrochemical methods on porous electrodes, we reviewed the recent literature on the electron transfer kinetics of the vanadium redox reactions on high surface area electrodes. As visualized in Fig. 5, the reported values for k_0 spread over four orders of magnitude. Scrutinizing a number of studies we found that several of them overestimated k_0 due to the apparent catalytic effect porous structures have on the peak position in CVs. Three studies that accounted for this fact or used alternative methods[17,65,79] find k_0 values from $9.1\ 10^{-7}\ cm\ s^{-1} < k_0 < 1.7\ 10^{-4} cm\ s^{-1}$ for VO^{2+}/VO_2^{+} and $2.4\ 10^{-7} cm\ s^{-1} < k_0 < 2.1\ 10^{-5}\ cm\ s^{-1}$ V^{2+}/V^{3+}. Of those three studies two investigated the influence of oxygen functional groups on the kinetics of the VO^{2+}/VO_2^{+} and find that these surface groups impede the kinetics[17,79]. It was therefore hypothesized that vanadium oxides chemisorb on the functional groups and thus passivate parts of the electrodes [13].

Also electrode ageing plays a significant role in VRB operation: Miller et al. showed that the positive effect of oxygen functional groups on the V^{2+}/V^{3+} redox reaction can likely not be maintained in actual VRB as the operating potential of the low potential half-cell leads to a deactivation of the electrode [79]. The low potential, or the evolved hydrogen, might reduce the functional groups that were thermally or chemically generated on the electrodes during pretreatment. This loss of functional groups slows the kinetics for the V^{2+}/V^{3+} redox reaction and diminishes the surface area of the electrode [13,76]. More pronounced ageing for the low potential half-cell was is also supported by results from Derr et al. who found that during cycling the negative half-cell shows a significant loss in performance whereas the positive half-cell remains stable [95]. However, their explanation was not the reduction of functional groups but chemical oxidation of the electrode which leads to a decrease in sp^2-hybridized carbon.

Electrochemical studies on the electron transfer constant k_0 yield important insights for the operation of electrochemical devices, exemplified here by the VRB. The correct investigation method has to be chosen for intrinsically complicated systems such as porous electrodes. EIS is a simple method that produces values for I_0 quickly. Alternatively, more intricate experimental methods can be employed to handle the problem of mass-transport limitations on porous electrodes [65,79]. However, equation 12 makes it obvious that increasing k_0 values in a RFB is only part of the optimization process. Besides the charge transfer overpotentials η_{ct} also the diffusion overpotentials η_{diff} and the ohmic resistances $I\,R_{Ohm}$ have to be understood and minimized to achieve efficient electrochemical energy storage in a RFB[24]. It is the challenge of electrochemical engineering to simultaneously minimize all three loss components in a scalable, efficient cell design. Especially the fundamentals of upscaling and cell stack designs are currently seen as impediment for the rollout of new technology[26,96,97].

References

(1) Béguin, F.; Presser, V.; Balducci, A.; Frackowiak, E. Carbons and Electrolytes for Advanced Supercapacitors. *Adv. Mater.* **2014**, 1–33.

(2) Chmiola, J.; Yushin, G.; Gogotsi, Y.; Portet, C.; Simon, P.; Taberna, P. L. Anomalous Increase in Carbon Capacitance at Pore Sizes Less than 1 Nanometer. *Science* **2006**, *313* (5794), 1760–1763.

(3) Mccreery, R. L. Advanced Carbon Electrode Materials for Molecular Electrochemistry. *Carbon N. Y.* **2008**, 2646–2687.

(4) Wolfschmidt, H.; Weingarth, D.; Stimming, U. Enhanced Reactivity for Hydrogen Reactions at Pt Nanoislands on Au(111). *Chemphyschem* **2010**, *11* (7), 1533–1541.

(5) Friedl, J.; Stimming, U. Model Catalyst Studies on Hydrogen and Ethanol Oxidation for Fuel Cells. *Electrochim. Acta* **2013**, *101*, 41–58.

(6) Hammer, B.; Norskov, J. B. Theoretical Surface Science and Catalysis — Calculations and Concepts. *Adv. Catal.* **2000**, *45*.

(7) Trasatti, S. Surface Science and Electrochemistry: Concepts and Problems. *Surf. Sci.* **1995**, *335*, 1–9.

(8) Chen, D.; Tao, Q.; Liao, L. W.; Liu, S. X.; Chen, Y. X.; Ye, S. Determining the Active Surface Area for Various Platinum Electrodes. *Electrocatalysis* **2011**, *2* (3), 207–219.

(9) Watt-Smith, M.; Friedrich, J.; Rigby, S.; Ralph, T.; Walsh, F. Determination of the Electrochemically Active Surface Area of Pt/C PEM Fuel Cell Electrodes Using Different Adsorbates. *J. Phys. D Appl. Phys.* **2008**, *41*, 1–8.

(10) Watt-Smith, M. J.; Rigby, S. P.; Ralph, T. R.; Walsh, F. C. Characterisation of Porous Carbon Electrode Materials Used in Proton Exchange Membrane Fuel Cells via Gas Adsorption. *J. Power Sources* **2008**, *184* (1), 29–37.

(11) Rice, R. J.; McCreery, R. L. Quantitative Relationship between Electron Transfer Rate and Surface Microstructure of Laser-Modified Graphite Electrodes. *Anal. Chem.* **1989**, *61* (15), 1637–1641.

(12) Rice, R. J.; Pontikos, N. M.; McCreery, R. L. Quantitative Correlations of Heterogeneous Electron-Transfer Kinetics with Surface Properties of Glassy Carbon Electrodes. *J. Am. Chem. Soc.* **1990**, *112* (12), 4617–4622.

(13) Fink, H.; Friedl, J.; Stimming, U. Composition of the Electrode Determines Which Half-Cell's Rate Constant Is Higher in a Vanadium Flow Battery. *J. Phys. Chem. C* **2016**, *120* (29), 15893–15901.

(14) Xu, W.; Zerda, T. W.; Raab, H.; Goritz, D. 3-D Morphological Characterization of Carbon Black Aggregates Using Atomic Force Microscopy. *Carbon N. Y.* **1997**, *35* (4), 471–474.

(15) Menshykau, D.; Streeter, I.; Compton, R. G. Influence of Electrode Roughness on Cyclic Voltammetry. *J. Phys. Chem. C* **2008**, *112* (37), 14428–14438.

(16) Punckt, C.; Pope, M.; Aksay, I. High Selectivity of Porous Graphene Electrodes Solely due to Transport and Pore Depletion Effects. *J. Phys. Chem. C* **2014**.

(17) Friedl, J.; Bauer, C. M.; Rinaldi, A.; Stimming, U. Electron Transfer Kinetics of the – Reaction on Multi-Walled Carbon Nanotubes. *Carbon N. Y.* **2013**, *63*, 228–239.

(18) Wadhawan, J. D.; Schro, U.; Neudeck, A.; Wilkins, S. J.; Compton, R. G.; Marken, F.; Consorti, C. S.; Souza, R. F. De. Ionic Liquid Modified Electrodes . Unusual Partitioning and in Droplet and Thin Layer Deposits Diffusion Effects of Fe (CN) 4 Tetrafluoroborate. *J. Electroanal. Chem.* **2000**, *493*, 75–83.

(19) Punckt, C.; Pope, M. A.; Liu, J.; Lin, Y.; Aksay, I. A. Electrochemical Performance of Graphene as Effected by Electrode Porosity and Graphene Functionalization. *Electroanalysis* **2010**, *22* (23), 2834–2841.

(20) Pumera, M. The Electrochemistry of Carbon Nanotubes: Fundamentals and Applications. *Chem. a Eur. J.* **2009**, *15* (20), 4970–4978.

(21) Keeley, G. P.; Lyons, M. E. G. The Effects of Thin Layer Diffusion at Glassy Carbon Electrodes Modified with Porous Films of Single-Walled Carbon Nanotubes. *J. Electrochem. Soc.* **2009**, *4*, 794–809.

(22) Goulet, M. A.; Skyllas-Kazacos, M.; Kjeang, E. The Importance of Wetting in Carbon Paper Electrodes for Vanadium Redox Reactions. *Carbon N. Y.* **2016**, *101*, 390–398.

(23) Starov, V. M.; Zhdanov, V. G. Effective Viscosity and Permeability of Porous Media. *Colloids Surfaces A Physicochem. Eng. Asp.* **2001**, *192* (1–3), 363–375.

(24) Watt-Smith, M. J.; Ridley, P.; Wills, R. G. A.; Shah, A. A.; Walsh, F. C. The Importance of Key Operational Variables and Electrolyte Monitoring to the Performance of an All Vanadium Redox Flow Battery. *J. Chem. Technol. Biotechnol.* **2013**, *88* (1), 126–138.

(25) Shah, A. A.; Watt-Smith, M. J.; Walsh, F. C. A Dynamic Performance Model for Redox-Flow Batteries Involving Soluble Species. *Electrochim. Acta* **2008**, *53* (27), 8087–8100.

(26) Walsh, F. C.; Pletcher, D. Electrochemical Engineering and Cell Design. In *Developments in Electrochemistry. Science inspired by Martin Felischmann*; Pletcher, D., Tian, Z.-Q., Williams, D. ., Eds.; John Wiley & Sons, 2014; pp 95–109.

(27) Ponce de Leon, C.; Friasferrer, A.; Gonzalezgarcia, J.; Szanto, D.; Walsh, F. Redox Flow Cells for Energy Conversion. *J. Power Sources* **2006**, *160* (1), 716–732.

(28) Weber, A. Z.; Mench, M. M.; Meyers, J. P.; Ross, P. N.; Gostick, J. T.; Liu, Q. Redox Flow Batteries: A Review. *J. Appl. Electrochem.* **2011**, *41* (10), 1137–1164.

(29) Aaron, D. S.; Liu, Q.; Tang, Z.; Grim, G. M.; Papandrew, A. B.; Turhan, A.; Zawodzinski, T. A.; Mench, M. M. Dramatic Performance Gains in Vanadium Redox Flow Batteries through Modified Cell Architecture. *J. Power Sources* **2012**, *206*, 450–453.

(30) Goulet, M.-A.; Ibrahim, O. A.; Kim, W. H. J.; Kjeang, E. Maximizing the Power Density of Aqueous Electrochemical Flow Cells with in Operando Deposition. *J. Power Sources* **2017**, *339*, 80–85.

(31) Skyllas-Kazacos, M.; Grossmith, F. Efficient Vanadium Redox Flow Cell. *J. Electrochem. Soc.* **1987**, *134* (12), 2950–2954.

(32) Weber, A. Z.; Mench, M. M.; Meyers, J. P.; Ross, P. N.; Gostick, J. T.; Liu, Q. Redox Flow Batteries: A Review. *J. Appl. Electrochem.* **2011**, *41* (10), 1137–1164.

(33) ORIJI, G. Investigation on V(IV)/V(V) Species in a Vanadium Redox Flow Battery. *Electrochim. Acta* **2004**, *49* (19), 3091–3095.

(34) Sum, E.; Rychcik, M.; Skyllas-Kazacos, M. Investigation of the V (V)/V (IV) System for Use in the Positive Half-Cell of a Redox Battery. *J. Power Sources* **1985**, *16*, 85–95.

(35) Agar, E.; Dennison, C. R.; Knehr, K. W.; Kumbur, E. C. Identification of Performance Limiting Electrode Using Asymmetric Cell Configuration in Vanadium Redox Flow Batteries. *J. Power Sources* **2013**, *225*, 89–94.

(36) Friedl, J. Advanced Materials for Redox Flow Batteries, Ph.D. Thesis, Technische Universitaet Muenchen, 2015.

(37) International Union of pure and applied Chemistry. *Standard Potentials in Aqueous Solution.*; Bard, A. J., Parsons, R., Jordan, J., Eds.; CRC Press: New York, 1985; Vol. 17.

(38) Bard, A.; Faulkner, L. *Electrochemical Methods: Fundamentals and Applications*, Second.; Harris, D., Swain, E., Robey, C., Aiello, E., Eds.; John Wiley and Sons: New York, 2001.

(39) Hawthorne, K. L.; Wainright, J. S.; Savinell, R. F. Studies of Iron-Ligand Complexes for an All-Iron Flow Battery Application. *J. Electrochem. Soc.* **2014**, *161* (10), A1662–A1671.

(40) Punckt, C.; Pope, M. A.; Aksay, I. A. On the Electrochemical Response of Porous Functionalized Graphene Electrodes. *J. Phys. Chem. C* **2013**, *117* (31), 16076–16086.

(41) Punckt, C.; Pope, M. A.; Liu, J.; Lin, Y.; Aksay, I. A. Electrochemical Performance of Graphene as Effected by Electrode Porosity and Graphene Functionalization. *Electroanalysis* **2010**, *22* (23), 2834–2841.

(42) Orazem, M.; Tribollet, B. *Electrochemical Impedance Spectroscopy*; John Wiley and Sons:

Hoboken, 2008.

(43) Hirschorn, B.; Orazem, M. E.; Tribollet, B.; Vivier, V.; Frateur, I.; Musiani, M. Determination of Effective Capacitance and Film Thickness from Constant-Phase-Element Parameters. *Electrochim. Acta* **2010**, *55* (21), 6218–6227.

(44) Yaeger, E.; Kuta, J. Techniques for the Study of Electrode Processes. In *Physical Chemistry. An advanced Treatise. Vol. IXA Electrochemistry*; Eyring, H., Ed.; Academic Press: New York/London, 1970; pp 346–451.

(45) Gnahm, M.; Pajkossy, T.; Kolb, D. M. The Interface between Au (111) and an Ionic Liquid. *Electrochim. Acta* **2010**, *55* (21), 6212–6217.

(46) Friedl, J.; Markovits, I. I. E.; Herpich, M.; Feng, G.; Kornyshev, A. A.; Stimming, U. Interface between an Au(111) Surface and an Ionic Liquid: The Influence of Water on the Double Layer Capacitance. *ChemElectroChem* **2016**, *71* (111), 311–315.

(47) Gerischer, H.; Vielstich, W. Zur Elektrolyse Bei Konstantem Elektrodenpotential. *Zeitschrift für Phys. Chemie* **1955**, *3*, 16–33.

(48) Hung, N. G.; Nagy, Z. Kinetics of the Ferrous/Ferric Electrode Reaction in the Absence of Chloride Catalysis. *J. Electrochem. Soc.* **1987**, *134* (9), 2215–2220.

(49) Gerischer, H. Eine Einführung in Die Methoden Zur Untersuchung Der Kinetik von Elektrodenprozessen. *Zeitschrift für Elektrochemie* **1955**, *50*, 604–612.

(50) Marcus, R. A. Exchange Reactions and Electron Transfer Reactions Including Isotopic Exchange. Theory of Oxidation-Reduction Reactions Involving Electron Transfer. Part 4.-A Statistical-Mechanical Basis for Treating Contributions from Solvent, Ligands, and Inert Salt. *Discuss. Faraday Soc.* **1960**, *29*, 21–31.

(51) Marcus, R. A.; Sutin, N. Electron Transfers in Chemistry and Biology. *Biochim. Biophys. Acta* **1985**, *811*, 265–322.

(52) Chidsey, C. E. Free Energy and Temperature Dependence of Electron Transfer at the Metal-Electrolyte Interface. *Science* **1991**, *251* (4996), 919–922.

(53) Henstridge, M. C.; Laborda, E.; Rees, N. V.; Compton, R. G. Marcus-Hush-Chidsey Theory of Electron Transfer Applied to Voltammetry: A Review. *Electrochim. Acta* **2012**, *84*, 12–20.

(54) Zeng, Y.; Smith, R.; Bai, P.; Bazant, M. Z. Simple Formula for Marcus-Hush-Chidsey Kinetics. **2014**, *735*, 1–16.

(55) Zeng, Y.; Bai, P.; Smith, R. B.; Bazant, M. Z. Simple Formula for Asymmetric Marcus-Hush Kinetics. *J. Electroanal. Chem.* **2015**, *748*, 52–57.

(56) Rosso, K. M.; Rustad, J. R. Ab Initio Calculation of Homogeneous Outer Sphere Electron Transfer Rates: Application to M(OH2)63+{&}{#}47;2+ Redox Couples. *J Phys Chem A* **2000**, *104* (29), 6718–6725.

(57) Bai, P.; Bazant, M. Z. Charge Transfer Kinetics at the Solid–solid Interface in Porous Electrodes. *Nat. Commun.* **2014**, *5*, 1–7.

(58) Tessonnier, J.-P.; Rosenthal, D.; Hansen, T. W.; Hess, C.; Schuster, M. E.; Blume, R.; Girgsdies, F.; Pfänder, N.; Timpe, O.; Su, D. S. Analysis of the Structure and Chemical Properties of Some Commercial Carbon Nanostructures. *Carbon N. Y.* **2009**, *47* (7), 1779–1798.

(59) Pletcher, D.; Walsh, F. C. Three-Dimensional Electrodes. In *Electrochemical Technology for a Cleaner Environment*; Genders, J. D., Weinberg, N. L., Eds.; The Electrosynthesis Company Inc.: New York, 1992.

(60) Friedl, J.; Bauer, C. M.; Rinaldi, A.; Stimming, U. Investigation of the Electron Transfer Kinetics of the VO2+/VO2+ -Reaction on Multi-Walled Carbon Nanotubes; p 3.

(61) Bockris, J. O.; Devanathan, M. A. V.; Mueller, K. On the Structure of Charged Interfaces. *Proc. R. Soc. Lond. A. Math. Phys. Sci.* **1963**, *274* (1356), 55–79.

(62) Parsons, R. The Rate of Electrolytic Hydrogen Evolution and the Heat of Adsorption of Hydrogen. *Trans. Faraday Soc.* **1958**, *54*, 1053–1063.

(63) Rampolla, R. W.; Miller, R. C.; Smyth, C. P. Microwave Absorption and Molecular Structure in Liquids. XXV. Measurements of Dielectric Constant and Loss at 3.1-Mm Wavelength by an Interferometric Method. *J. Chem. Phys.* **1959**, *30* (2), 566–573.

(64) Cooper, J. A.; Compton, R. G. Channel Electrodes — A Review. *Electroanalysis* **1998**, *10* (3), 141–155.

(65) Goulet, M.-A.; Eikerling, M.; Kjeang, E. Direct Measurement of Electrochemical Reaction Kinetics in Flow-through Porous Electrodes. *Electrochem. commun.* **2015**, *57*, 14–17.

(66) Vetter, K. J. *Electrochemical Kinetics - Theoretical and Experimental Aspects*, English Ed.; Academic Press Inc.: New York/London, 1967.

(67) Birkin, P. R.; Silva-Martinez, S. Determination of Heterogeneous Electron Transfer Kinetics in the Presence of Ultrasound at Microelectrodes Employing Sampled Voltammetry. *Anal. Chem.* **1997**, *69* (11), 2055–2062.

(68) Gattrell, M.; Park, J.; MacDougall, B.; Apte, J.; McCarthy, S.; Wu, C. W. Study of the Mechanism of the Vanadium 4+/5+ Redox Reaction in Acidic Solutions. *J. Electrochem. Soc.* **2004**, *151* (1), A123.

(69) Bourke, A.; Lynch, R. P.; Buckley, D. N. Effect of Electrode Pretreatment on the Cyclic

Voltammetry of VO2+/VO2+ at a Glassy Carbon Electrode. *ECS Trans.* **2013**, *53* (30), 59–67.

(70) Bourke, A.; Quill, N.; Lynch, R. P.; Buckley, D. N. Effect of Pretreatment on the Rate of the VO2+/VO2+ and V2+/V3+ Reactions at a Carbon Electrode. *ECS Trans.* **2014**, *61* (37), 15–26.

(71) Chakrabarti, M. H.; Brandon, N. P.; Hajimolana, S. A.; Tariq, F.; Yufit, V.; Hashim, M. A.; Hussain, M. A.; Low, C. T. J.; Aravind, P. V. Application of Carbon Materials in Redox Flow Batteries. *J. Power Sources* **2014**, *253*, 150–166.

(72) Yao, C.; Zhang, H.; Liu, T.; Li, X.; Liu, Z. Carbon Paper Coated with Supported Tungsten Trioxide as Novel Electrode for All-Vanadium Flow Battery. *J. Power Sources* **2012**, *218*, 455–461.

(73) Pour, N.; Kwabi, D. G.; Carney, T. J.; Darling, R. M.; Perry, M. L.; Shao-Horn, Y. Influence of Edge- and Basal-Plane Sites on the Vanadium Redox Kinetics for Flow Batteries. *J. Phys. Chem. C* **2015**, No. 2, 150216172359004.

(74) Aaron, D.; Sun, C.-N.; Bright, M.; Papandrew, a. B.; Mench, M. M.; Zawodzinski, T. a. In Situ Kinetics Studies in All-Vanadium Redox Flow Batteries. *ECS Electrochem. Lett.* **2013**, *2* (3), A29–A31.

(75) Noack, J.; Roznyatovskaya, N.; Herr, T.; Fischer, P. The Chemistry of Redox-Flow Batteries. *Angew. Chemie Int. Ed.* **2015**, *54* (34), 9776–9809.

(76) Langner, J.; Bruns, M.; Dixon, D.; Nefedov, A.; Wöll, C.; Scheiba, F.; Ehrenberg, H.; Roth, C.; Melke, J. Surface Properties and Graphitization of Polyacrylonitrile Based Fiber Electrodes Affecting the Negative Half-Cell Reaction in Vanadium Redox Flow Batteries. *J. Power Sources* **2016**, *321*, 210–218.

(77) Steimecke, M.; Rümmler, S.; Kühhirt, M.; Bron, M. A Linear Sweep Voltammetric Procedure Applied to Scanning Electrochemical Microscopy for the Characterization of Carbon Materials

towards the Vanadium(IV)/(V) Redox System. *ChemElectroChem* **2016**, *3* (2), 318–322.

(78) Jelyani, M. Z.; Rashid-Nadimi, S.; Asghari, S. Treated Carbon Felt as Electrode Material in Vanadium Redox Flow Batteries: A Study of the Use of Carbon Nanotubes as Electrocatalyst. *J. Solid State Electrochem.* **2016**, No. DOI 10.1007/s10008-016-3336-y.

(79) Miller, M. A.; Bourke, A.; Quill, N.; Wainright, J. S.; Lynch, R. P.; Buckley, D. N.; Savinell, R. F. Kinetic Study of Electrochemical Treatment of Carbon Fiber Microelectrodes Leading to In Situ Enhancement of Vanadium Flow Battery Efficiency. *J. Electrochem. Soc.* **2016**, *163* (9), A2095–A2102.

(80) Schweiss, R. Influence of Bulk Fibre Properties of PAN-Based Carbon Felts on Their Performance in Vanadium Redox Flow Batteries. *J. Power Sources* **2015**, *278*, 308–313.

(81) Wu, X. W.; Yamamura, T.; Ohta, S.; Zhang, Q. X.; Lv, F. C.; Liu, C. M.; Shirasaki, K.; Satoh, I.; Shikama, T.; Lu, D.; et al. Acceleration of the Redox Kinetics of VO2+/VO2 + and V3+/V2+ Couples on Carbon Paper. *J. Appl. Electrochem.* **2011**, *41* (10), 1183–1190.

(82) Mazurenko, I.; Etienne, M.; Francius, G.; Vakulko, I.; Walcarius, A. Macroporous Carbon Nanotube-Carbon Composite Electrodes. *Carbon N. Y.* **2016**.

(83) Rabbow, T. J.; Trampert, M.; Pokorny, P.; Binder, P.; Whitehead, A. H. Variability within a Single Type of Polyacrylonitrile-Based Graphite Felt after Thermal Treatment. Part I: Physical Properties. *Electrochim. Acta* **2015**, *173*, 17–23.

(84) Rabbow, T. J.; Trampert, M.; Pokorny, P.; Binder, P.; Whitehead, A. H. Variability within a Single Type of Polyacrylonitrile-Based Graphite Felt after Thermal Treatment. Part II: Chemical Properties. *Electrochim. Acta* **2015**, *173*, 24–30.

(85) Zhang, J.; Zou, H.; Qing, Q.; Yang, Y.; Li, Q. Effect of Chemical Oxidation on the Structure of Single-

Walled Carbon Nanotubes. *J. Phys. Chem. B* **2003**, *107* (16), 3712–3718.

(86) Rinaldi, A. Synthesis of Carbon Nanotubes on Carbon Supports and the Purification of Carbon Nanotubes, Technische Universitaet Berlin, 2010.

(87) Ros, T. G.; van Dillen, A. J.; Geus, J. W.; Koningsberger, D. C. Surface Oxidation of Carbon Nanofibres. *Chem. a Eur. J.* **2002**, *8* (5), 1151–1162.

(88) Zielke, U.; Hüttinger, K. J.; Hoffman, W. P. Surface Oxidized Carbon Fibers: I. Surface Structure and Chemistry. *Carbon N. Y.* **1996**, *34* (8), 983–998.

(89) LI, L.; LI, F. The Effect of Carbonyl, Carboxyl and Hydroxyl Groups on the Capacitance of Carbon Nanotubes. *New Carbon Mater.* **2011**, *26* (3), 224–228.

(90) Gattrell, M.; Qian, J.; Stewart, C.; Graham, P.; MacDougall, B. The Electrochemical Reduction of VO2+ in Acidic Solution at High Overpotentials. *Electrochim. Acta* **2005**, *51* (3), 395–407.

(91) Melke, J.; Jakes, P.; Langner, J.; Riekehr, L.; Kunz, U.; Zhao-Karger, Z.; Nefedov, A.; Sezen, H.; Wöll, C.; Ehrenberg, H.; et al. Carbon Materials for the Positive Electrode in All-Vanadium Redox Flow Batteries. *Carbon N. Y.* **2014**, *78*, 220–230.

(92) Park, M.; Ryu, J.; Kim, Y.; Cho, J. Corn Protein-Derived Nitrogen-Doped Carbon Materials with Oxygen-Rich Functional Groups: A Highly Efficient Electrocatalyst for All-Vanadium Redox Flow Batteries. *Energy Environ. Sci.* **2014**, *7* (11), 3727–3735.

(93) Yamamura, T.; Watanabe, N.; Yano, T.; Shiokawa, Y. Electron-Transfer Kinetics of Np3+/Np4+, NpO2+/NpO22+, V2+/V3+, and VO2+/VO2+ at Carbon Electrodes. *J. Electrochem. Soc.* **2005**, *152* (4), A830.

(94) Maruyama, J.; Shinagawa, T.; Hayashida, A.; Matsuo, Y.; Nishihara, H.; Kyotani, T. Vanadium-Ion

Redox Reactions in a Three-Dimensional Network of Reduced Graphite Oxide. *ChemElectroChem* **2016**, *3* (4), 650–657.

(95) Derr, I.; Bruns, M.; Langner, J.; Fetyan, A.; Melke, J.; Roth, C. Degradation of All-Vanadium Redox Flow Batteries (VRFB) Investigated by Electrochemical Impedance and X-Ray Photoelectron Spectroscopy: Part 2 Electrochemical Degradation. *J. Power Sources* **2016**, *325*, 351–359.

(96) Marshall, R. J.; Walsh, F. C. A Review of Some Recent Electrolytic Cell Designs. *Surf. Technol.* **1985**, *24* (1), 45–77.

(97) Walsh, F. C. Electrochemical Technology for Environmental Treatment and Clean Energy Conversion. *Pure Appl. Chem.* **2001**, *73* (12), 1819–1837.

Figure 1 *Cyclic voltammograms of 50 mM Fe^{2+} and 50 mM Fe^{3+}. (a) Experimental curves on a GC electrode (orange curve), GC electrode with 1 µg of MWCNTs (green curve) and 4 µg of MWCNTs (blue curve). (b) Calculated CVs for two systems. The surface area of system 2 (blue curve) is ten times higher and its diffusion coefficient is 100 times lower than that of system 1 (orange curve). All parameters are given in the graph. (c) Cartoon of a porous carbon structure on a flat electrode. The porous surface area that will have a small diffusion coefficient compared to the freely accessible electrode area (orange) is marked blue.*

Figure 2 *(a) Cyclic voltammograms of 50 mM Fe^{2+} and 50 mM Fe^{3+}on a GC electrode with 4 µg of MWCNTs recorded at various scan-speeds. The current density was divided by the square-root of the scan-speed. (b) Peak separation over scan speed for electrodes with 1 and 4 µg MWCNTs (c) Simulated electron transfer constants over scan speed for electrodes with 1 and 4 µg MWCNTs.*

Figure 3 *(a) Nyquist representation and (b) Bode plot of 50 mM Fe^{2+} and 50 mM Fe^{3+} on a GC electrode with 1 µg of MWCNTs. The fit results with their errors are given.*

Figure 4 *(a) Chronoamperometry curves for 50 mM Fe^{2+} and 50 mM Fe^{3+} on a GC electrode with 1 µg of MWCNTs for various anodic overpotentials. (b) Extrapolated absolute current values at t = 0s vs. overpotential. The analysis is done following the Butler-Volmer (BV) and the Marcus-Hush-Chidsey (MHC) model.*

Figure 5 *Electron transfer constants on various porous carbon electrodes listed in Table 2. Electrodes were selected and grouped into three categories: oxidized, untreated and reduced. (a) VO^{2+}/VO_2^{+} redox reaction. (b) V^{2+}/V^{3+} redox reaction.*

Figure 6 *Inverse charge transfer resistance R_{CT}^{-1} over double layer capacitance C_{DL} for three CNT samples. The data points are fitted linearly and the slopes are given in the legend. Data from* [17].

Method	$I_0 \ / \ mA$	$k_0^{CDL} / cm\ s^{-1}$	$k_0^{BET} / cm\ s^{-1}$
Electrochemical impedance spectroscopy	2.3 ± 0.5	$(1.1 \pm 0.2)\ 10^{-4}$	$(1.2 \pm 0.2)\ 10^{-4}$
Chronoamperometry BV	1.5 ± 0.45	$(6.7 \pm 2.0)\ 10^{-5}$	$(7.6 \pm 2.3) 10^{-5}$
Chronoamperometry MHC	1.6 ± 0.13	$(7.1 \pm 0.6)\ 10^{-5}$	$(8.1 \pm 0.7)\ 10^{-5}$

Table 1: *Kinetic information for Fe^{2+}/Fe^{3+} extracted from EIS and CA. Results from CA were fitted by the Butler-Volmer and the Marcus-Hush-Chidsey model.*

Electrode	Method	Surface area	k_0 (VO^{2+}/VO_2^+) / cm s^{-1}	k_0 (V^{2+}/V^{3+}) / cm s^{-1}	Ref
CF loaded with CNTs, acid and heat treated (AH)	(CV), EIS	geometric	CF: 1.1 10^{-5} CNT+ CF: 4.6 10^{-5} CNT+ CF AH: 1.1 10^{-3}	CF: 7.4 10^{-6} CNT+ CF: 7.2 10^{-5} CNT+ CF AH: 1.3 10^{-3}	[55]
CFME, oxidized (1.5 V vs. MSE) and reduced (-2.0 V vs. MSE)	LSV, EIS	geometric, SEM	CFME ox. (LSV): 1.7 10^{-5} CFME red. (LSV): 7.3 10^{-5} CFME ox. (EIS): 3.6 10^{-5} CFME red. (EIS): 1.7 10^{-4}	CFME ox. (LSV): 5.8 10^{-6} CFME red. (LSV): 6.0 10^{-7} CFME ox. (EIS): 2.1 10^{-5} CFME red. (EIS): 1.0 10^{-6}	[56]
CP	LSV flow cell, (EIS)	Mercury intrusion porosimetry	1.8 10^{-5}	2.4 10^{-7}	[57]
CNTs pristine, acid treated and defunctionalized	(CV), EIS	C_{DL} from EIS	CNT pristine: 1.8 10^{-6} CNT acid: 9.1 10^{-7} CNT defunc.: 3.8 10^{-6}		[14]
CFs, Sigracell GFD4.6	CV	BET	GFD 4.6: 6.2 10^{-5}	GFD 4.6: 1 10^{-6}	[58]
CF pristine, acid and heat treated	CV	geometric	CF pristine$^+$: 1.4 10^{-5} CF acid$^+$: 2.0 10^{-5} CF heat$^+$: 3.0 10^{-5}	CF pristine: 1.54 10^{-5} CF acid: 4.6 10^{-5} CF heat$^+$: 6.9 10^{-5}	[25]
CP	CV	BET	1.0 10^{-3}	1.1 10^{-3}	[59]
CNT with carbon binder	CV	Randles-Sevcik	CNT treated at 650 ˚C: 1.3 10^{-3}		[60]

		equation CV			

Table 2 *Studies that give values for the vanadium redox reactions on porous carbon materials. CF – carbon fiber, CNT – carbon nanotube, CFME – carbon fiber microelectrode, CP – carbon paper, LSV – linear sweep voltammetry, SEM –Scanning electron microscopy, BET – Brunauer-Emmett-Teller. A method in bracket means that an electrochemical method was performed but not used to extract kinetic information.* $^{+}$ *calculated as the arithmetic mean of forward and backward reaction.*

Figure 1

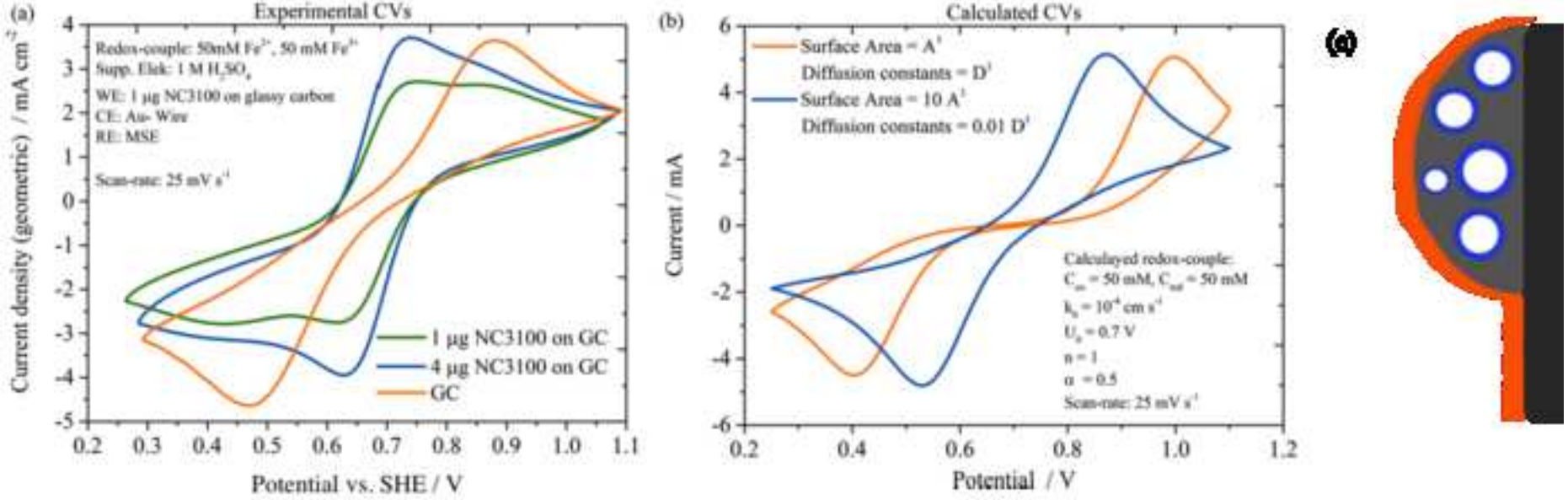
(a)
Experimental CVs
Redox-couple: 50mM Fe2+, 50 mM Fe3+
Supp. Elek: 1 M H2SO4
WE: 1 µg NC3100 on glassy carbon
CE: Au- Wire
RE: MSE
Scan-rate: 25 mV s-1
1 µg NC3100 on GC
4 µg NC3100 on GC
GC
Current density (geometric) / mA cm-2
Potential vs. SHE / V
(b)
Calculated CVs
Surface Area = A1
Diffusion constants = D1
Surface Area = 10 A1
Diffusion constants = 0.01 D1
Calculated redox-couple:
Cox = 50 mM, Cred = 50 mM
k0 = 10-4 cm s-1
U0 = 0.7 V
n = 1
α = 0.5
Scan-rate: 25 mV s-1
Current / mA
Potential / V
(c)

Figure 2

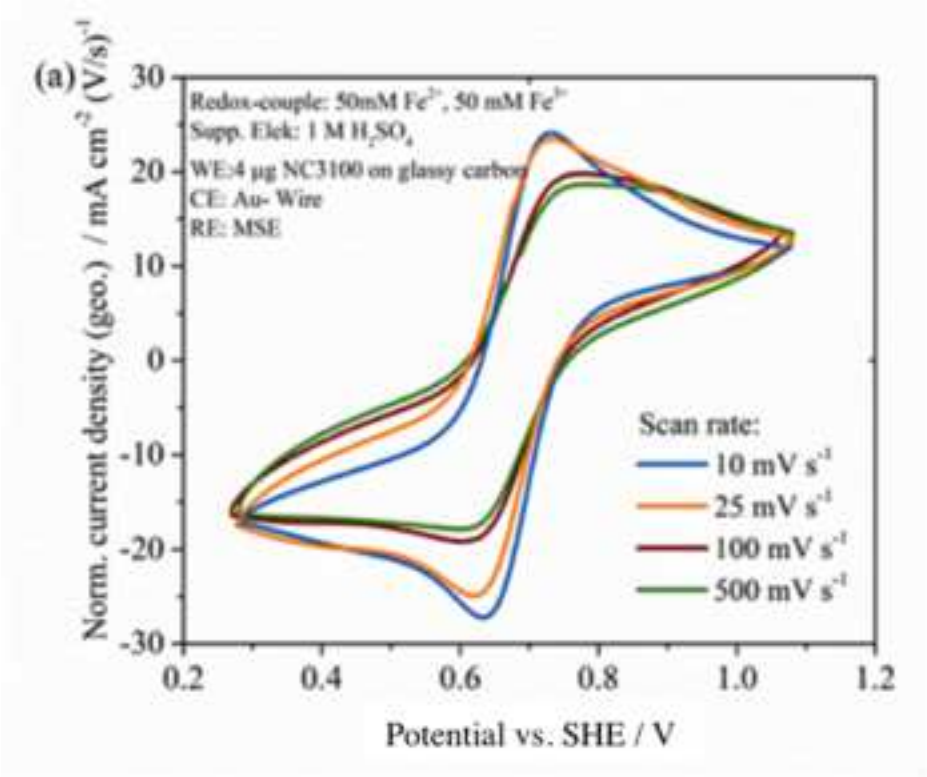
(a)
Redox-couple: 50mM Fe2+, 50 mM Fe3+
Supp. Elek: 1 M H2SO4
WE:4 µg NC3100 on glassy carbon
CE: Au- Wire
RE: MSE
Scan rate:
10 mV s-1
25 mV s-1
100 mV s-1
500 mV s-1
Norm. current density (geo.) / mA cm-2 (V/s)-1
Potential vs. SHE / V

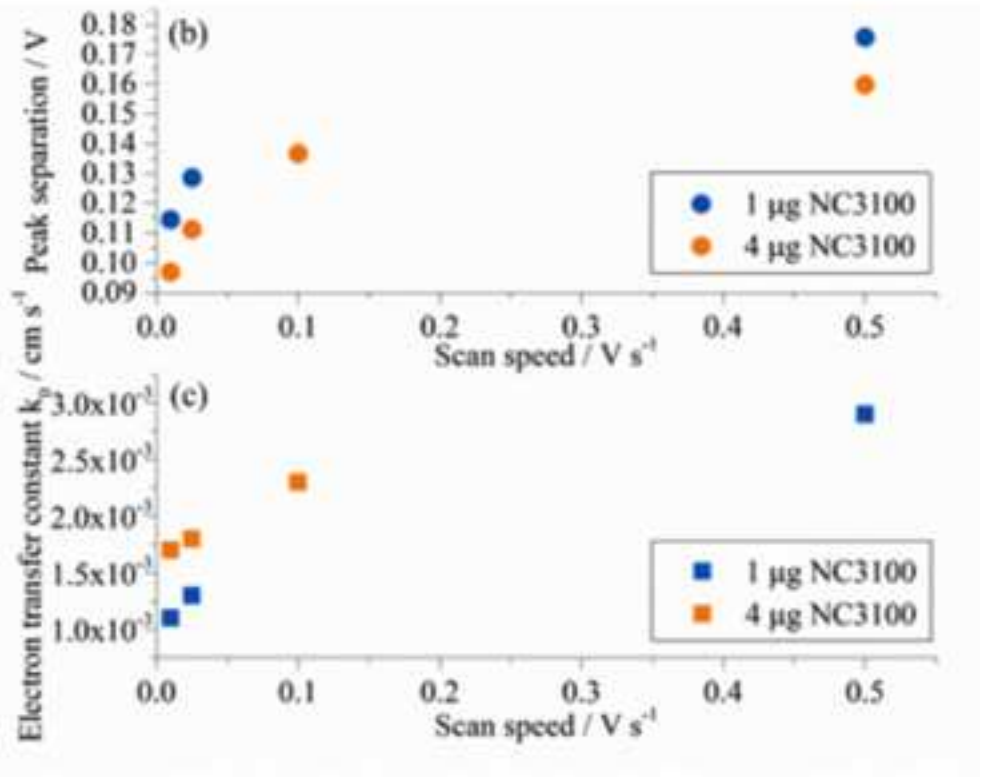
(b)
Peak separation / V
Scan speed / V s-1
1 µg NC3100
4 µg NC3100
(c)
Electron transfer constant kp / cm s-1
Scan speed / V s-1
1 µg NC3100
4 µg NC3100

Figure 3

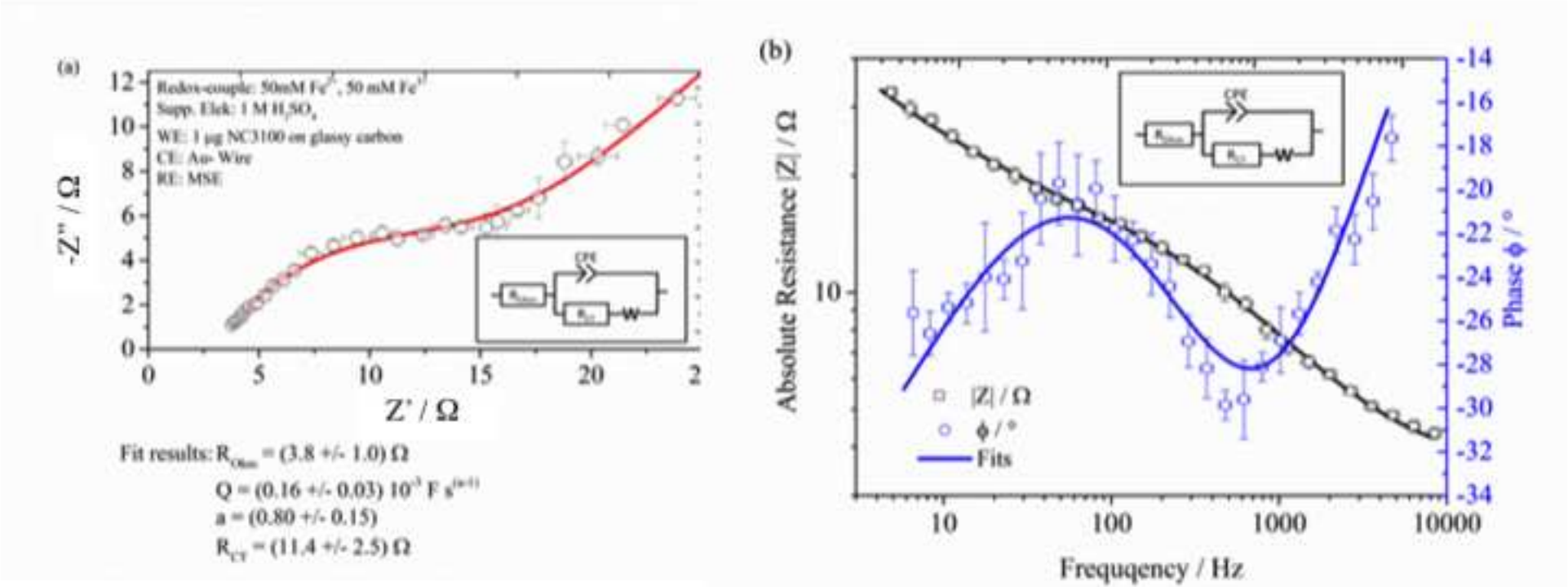
(a)
Redox-couple: 50mM Fe2+, 50 mM Fe3+
Supp. Elek: 1 M H2SO4
WE: 1 µg NC3100 on glassy carbon
CE: Au- Wire
RE: MSE
-Z'' / Ω
Z' / Ω
CPE
W
Fit results: R = (3.8 +/- 1.0) Ω
Q = (0.16 +/- 0.03) 10-3 F s(a-1)
a = (0.80 +/- 0.15)
RCT = (11.4 +/- 2.5) Ω
(b)
Absolute Resistance |Z| / Ω
Phase ϕ / °
|Z| / Ω
ϕ / °
Fits
Frequqency / Hz

Figure 4

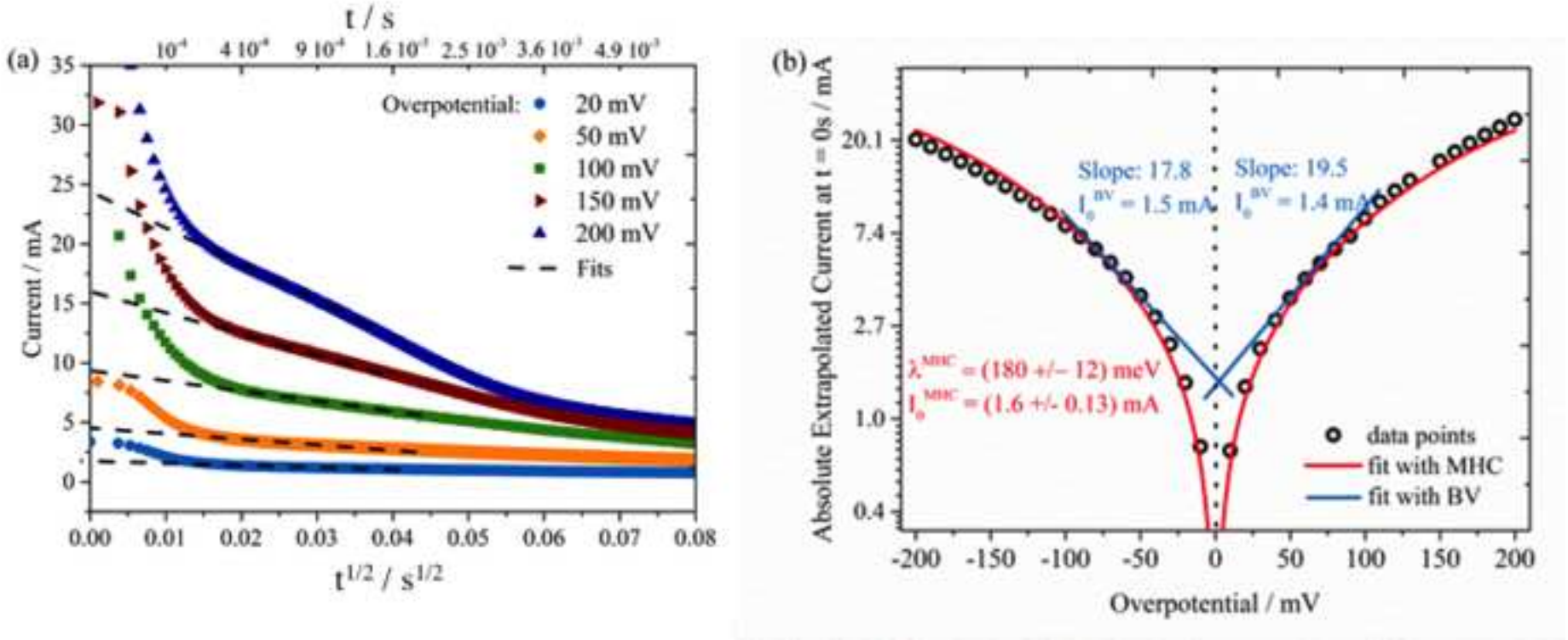
(a)
t / s
10⁻⁴ 4 10⁻⁴ 9 10⁻⁴ 1.6 10⁻³ 2.5 10⁻³ 3.6 10⁻³ 4.9 10⁻³
Overpotential:
20 mV
50 mV
100 mV
150 mV
200 mV
Fits
Current / mA
t^1/2 / s^1/2
(b)
Absolute Extrapolated Current at t = 0s / mA
Slope: 17.8
Slope: 19.5
λ^MHC = (180 +/– 12) meV
I_o^MHC = (1.6 +/- 0.13) mA
data points
fit with MHC
fit with BV
Overpotential / mV

Figure 5

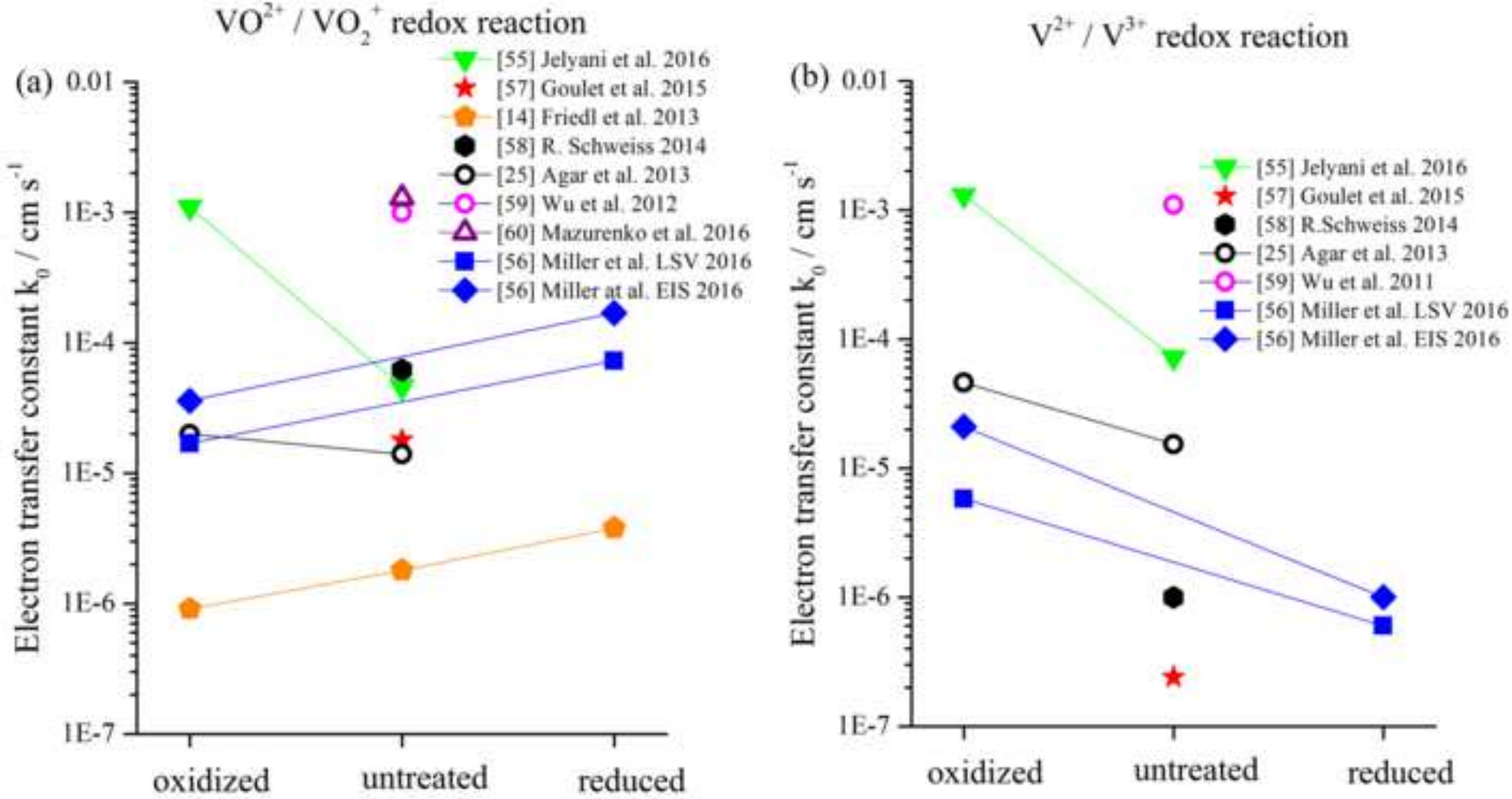
(a)
VO2+ / VO2+ redox reaction
Electron transfer constant k0 / cm s-1
0.01
1E-3
1E-4
1E-5
1E-6
1E-7
oxidized
untreated
reduced
[55] Jelyani et al. 2016
[57] Goulet et al. 2015
[14] Friedl et al. 2013
[58] R. Schweiss 2014
[25] Agar et al. 2013
[59] Wu et al. 2012
[60] Mazurenko et al. 2016
[56] Miller et al. LSV 2016
[56] Miller at al. EIS 2016
(b)
V2+ / V3+ redox reaction
Electron transfer constant k0 / cm s-1
0.01
1E-3
1E-4
1E-5
1E-6
1E-7
oxidized
untreated
reduced
[55] Jelyani et al. 2016
[57] Goulet et al. 2015
[58] R.Schweiss 2014
[25] Agar et al. 2013
[59] Wu et al. 2011
[56] Miller et al. LSV 2016
[56] Miller et al. EIS 2016

Figure 6

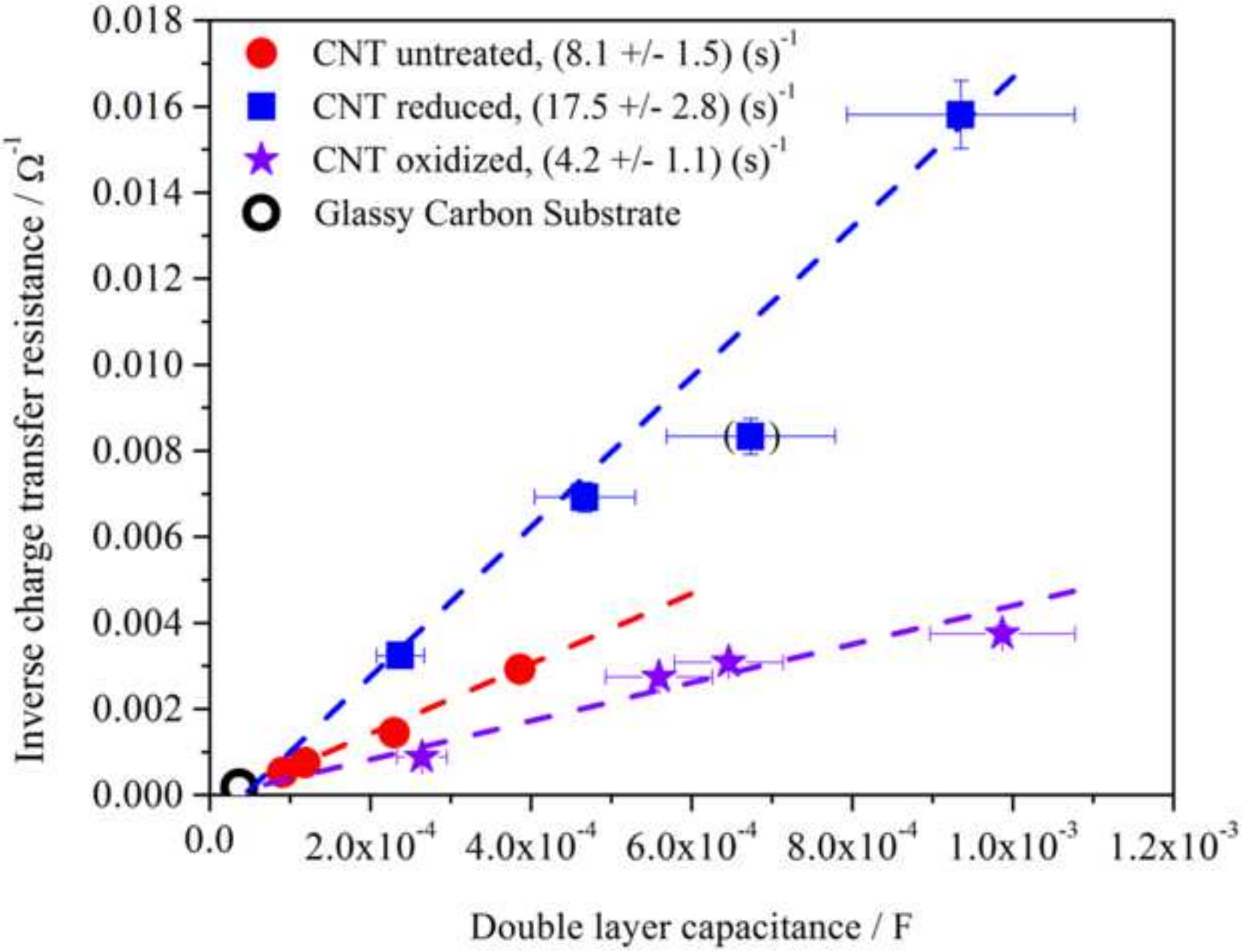
CNT untreated, (8.1 +/- 1.5) (s)-1
CNT reduced, (17.5 +/- 2.8) (s)-1
CNT oxidized, (4.2 +/- 1.1) (s)-1
Glassy Carbon Substrate
Inverse charge transfer resistance / Ω-1
Double layer capacitance / F
0.000
0.002
0.004
0.006
0.008
0.010
0.012
0.014
0.016
0.018
0.0
2.0x10-4
4.0x10-4
6.0x10-4
8.0x10-4
1.0x10-3
1.2x10-3